THE JOURNAL OF PHYSICAL CHEMISTRY B

Article

Cite This: J. Phys. Chem. B 2019, 123, 9984−9991

pubs.acs.org/JPCB

Papain Adsorption on Latex Particles: Charging, Aggregation, and Enzymatic Activity

Szilárd Sáringer, Rita Achieng Akula, Adél Szerlauth, and Istvan Szilagyi*

MTA-SZTE Lendület Biocolloids Research Group, Interdisciplinary Excellence Center, Department of Physical Chemistry and Materials Science, University of Szeged, 1 Rerrich Béla tér, H-6720 Szeged, Hungary

ABSTRACT: The effect of papain adsorption on the surface charge properties and aggregation mechanism of sulfate-functionalized polystyrene latex particles was studied. The positively charged enzyme possessed a high affinity to the oppositely charged particles, giving rise to charge neutralization and charge reversal at appropriate papain concentrations. The tendency in the particle aggregation rates at different enzyme doses revealed that the colloidal stability of the samples is governed by interparticle forces of electrostatic origin. The aggregation mechanism was qualitatively described within the classical DLVO theory, and unstable dispersions were detected near the charge neutralization point, while particle aggregation was not observed at low and elevated papain concentrations. The relatively high dispersion stability of the bare latex particles was maintained upon the formation of an enzyme layer on the surface, and the obtained latex−papain composite showed notable resistance against salt-induced aggregation. Remarkable hydrolytic and antioxidant activities of the immobilized enzyme were observed in probe reactions; therefore, the obtained hybrid can be considered as a multifunctional biocatalytic system with great promise in applications in industrial manufacturing processes.

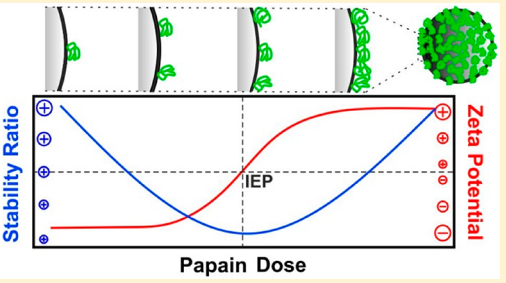

INTRODUCTION

Enzyme immobilization attracts widespread contemporary interest due to the progressively growing number of applications, where biocatalytic systems are involved in maintaining green and sustainable chemical manufacturing processes.[1−3] Various immobilization techniques including covalent grafting, physical adsorption, and enzyme entrapment were developed in the past to attach the proteins to the solid supports in order to achieve a high yield, long functional stability, and good selectivity.[4] Considerable effort was made to design and synthesize solid supports of advantageous chemical and physical properties; therefore, silica,[5] clays,[6] carbon derivatives,[7,8] polymeric substances,[9,10] titania,[11] and organic−inorganic hybrid materials[12,13] were applied to immobilize enzymes.

Among the enzyme families involved in immobilization processes, proteases represent an important class due to their widespread applications in the food, detergent, and pharmaceutical industries.[14] They hydrolyze amide bonds and, hence, convert long-chain proteins to peptides and subsequently to amino acids. This process is highly utilized in meat tenderization, beer clarification, and softening of cheese. As a prominent representative of the group proteases, the papain enzyme is widely used in the above applications.[15] Its main advantage over other proteases includes good hydrolytic activity against a broad range of protein substrates and that it can be produced in a considerable amount from the fruit of the papaya tree.[16] Apart from acting as a protease, papain showed remarkable antioxidant activity;[17] therefore, its utilization in chemical manufacturing processes in the food industry is highly advantageous. Nevertheless, the use of native papain is often complicated, and thus, immobilization is highly recommended to improve stability, to achieve better recyclability, and to separate the enzyme from the reaction mixture after the catalytic process is terminated.

Accordingly, papain was immobilized on magnetic nanoparticles prepared by polymerization of methacrylate containing monomers in the presence of iron oxide powder.[18] To enhance the enzymatic affinity, the surface of the support was decorated by dye ligands, giving rise to remarkable enzyme loading into the nanoparticles. The immobilized papain showed excellent activity and stability in the hydrolytic decomposition of various proteins. In another system, papain was intercalated into layered double hydroxide nanoparticles in a coprecipitation synthesis carried out in the presence of the enzyme.[19] The papain attained a compressed conformation in the interlayer space; however, the original structure was recovered after releasing the enzyme from the host material, indicating a promising papain delivery system. Attachment of the enzyme to a hydrogel composite consisting of a cellulose derivative, polyalcohol, and silica particles led to a remarkable increment in the long term stability compared to the free enzyme.[20] Similar improvement was achieved in the functional stability once papain was covalently grafted to nanocomposites of gold, magnetite, and cellulose.[21] This material was used for the development of electrochemical sensors for peptide

Received: September 16, 2019
Revised: October 26, 2019
Published: October 31, 2019

DOI: 10.1021/acs.jpcb.9b08799
J. Phys. Chem. B 2019, 123, 9984−9991

detection. In addition, papain was embedded within polyelectrolyte−clay layers using the sequential adsorption method. However, the layered structure possessed limited stability, and enzyme leakage was detected.[22]

The above-discussed host−guest materials and also other papain−solid support hybrids are mainly used in heterogeneous systems; i.e., the hybrid materials are dispersed in liquid media. To achieve good catalytic performance, stable dispersions containing homogeneously distributed primary particles of high surface area are required, while the catalysts can be removed from the reaction mixture by particle aggregation and subsequent sedimentation or filtration. These facts highlight the importance of the colloidal stability of such systems. Indeed, it was pointed out earlier that protein adsorption on nanoparticles significantly changes the surface charge behavior of the solid supports, leading to a notable variation in the speed of particle aggregation.[23−25] For instance, the size of gold nanoparticle aggregates can be controlled by protein adsorption.[26] In addition, similar gold nanoparticles were prepared with a lysozyme monolayer on their surface, giving rise to the development of a biocompatible nanocomposite of excellent colloidal stability.[27] However, to the best of our knowledge, no studies on the influence of papain functionalization on the stability of the dispersions of particle supports were reported in the past.

Therefore, the aim of the present work was to investigate the effect of papain adsorption on the colloidal stability of polystyrene latex particles in oppositely charged systems; i.e., positively charged enzyme and negatively charged particles were present in the experiments due to the careful adjustment of the experimental conditions. The charging behavior and the aggregation processes were explored at different papain concentrations and ionic strengths with light scattering techniques. The possible change in the enzymatic activity upon immobilization was investigated in biochemical test reactions.

EXPERIMENTAL SECTION

Materials. Spherical polystyrene latex particles were purchased from Thermo Fischer Scientific. The size was 430 nm in diameter with a coefficient of variation of 1.8%, as determined by the manufacturer using transmission electron microscopy (TEM) in the dried stage. The surface of the particles was functionalized with negatively charged sulfate groups, leading to a surface charge density of −12 mC/m^2 provided on the basis of potentiometric titration by the company. Papain from Carica papaya was purchased from Sigma-Aldrich in powder form with ≥3 U/mg. Hydrogen chloride (HCl), sodium chloride (NaCl), sodium acetate, sodium carbonate anhydrous, calcium acetate, sodium phosphate monobasic anhydrous, disodium hydrogen phosphate anhydrous, dipotassium hydrogen orthophosphate trihydrate, casein, trichloroacetic acid (TCA), and methanol were purchased from VWR, while Folin & Ciocalteu's reagent was bought from Sigma-Aldrich. The 2,2-diphenyl-1-picrylhydrazyl (DPPH) was purchased from Alfa Aesar. These chemicals were analytical grade and used as received. All solutions were diluted using ultrapure water obtained from the VWR purity TU+ machine. The water and the salt solutions were filtered with a 0.1 μm syringe filter (Millex).

Light Scattering. Dynamic light scattering (DLS) experiments were performed in time-resolved mode on an ALV-NIBS High-Performance Particle Sizer equipped with a 3 mW He−Ne laser with a 633 nm wavelength. The correlation function was acquired during 20 s, and 100−250 runs were performed in the measurements depending on the speed of aggregation. To determine the particle size, a second cumulant fit was applied to the correlation function, and the Stokes−Einstein equation was used for the conversion of the diffusion coefficient to the hydrodynamic radius (R_h).[28,29] During sample preparation, 2 mL dispersions were prepared. The particle concentration, ionic strength, and enzyme dose were adjusted by mixing appropriate amounts of stock solutions. The time-resolved measurements were initiated by adding the latex sample to the electrolyte−enzyme mixture. The experiments were carried out at 25 °C.

To study the early stages of particle aggregation, where mainly dimers form and no higher ranked aggregates are present in the samples, the experimental conditions were optimized by performing time-resolved DLS experiments in 1 M NaCl solutions at different particle concentrations (Figure 1). The apparent aggregation rates (k_{app}) were calculated from these measurements as

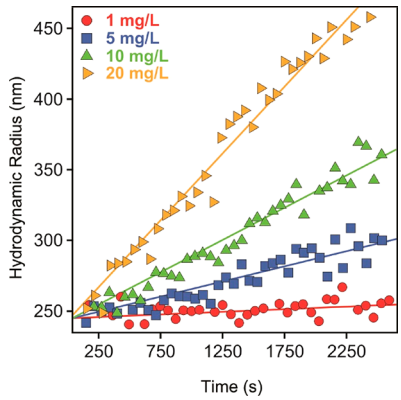

Figure 1. Particle concentration dependence (sulfate latex particles in 1 M NaCl) on the slopes of the hydrodynamic radius versus time plots. The solid lines are linear fits used to calculate the apparent aggregation rates in eq 1.

$$k_{app} = \frac{1}{R_h^0}\frac{dR_h}{dt}\bigg|_{t\to 0} \quad (1)$$

where R_h^0 is the hydrodynamic radius of the monomers, which was measured by DLS as 236 nm in stable dispersions. This value is somewhat higher than the geometrical radius determined by TEM (215 nm) due to the finite polydispersity of the particles and to the different environments during the DLS and TEM measurements. At such a high salt level, the aggregation is driven solely by the diffusion of the particles. On the basis of the k_{app} data, a particle concentration of 10 mg/L was chosen for further experiments. This value gives a good compromise that the aggregation is in its early stage, the measurement time is reasonable, and the scattered intensity is high enough to perform accurate DLS measurements.

The absolute aggregation rate coefficient of dimer formation (k) was determined at the above particle concentration in 1 M NaCl solution as[30]

DOI: 10.1021/acs.jpcb.9b08799
J. Phys. Chem. B 2019, 123, 9984−9991

$$k = \frac{k_{app}}{\left(1 + \frac{\sin(2qR)}{2qR}\right)\left(1 - \frac{R_{h1}}{R_{h2}}\right)N_0} \quad (2)$$

where R is the geometrical radius of the particles, N_0 is the initial particle concentration, q is the scattering vector,[29] and R_{h1} and R_{h2} are the hydrodynamic radius of the monomer and dimer, respectively. The R_{h2}/R_{h1} ratio was reported to be 1.38.[31] Equation 2 assumes the validity of the Rayleigh−Gans−Debye approximation for the form factor, as it was demonstrated to be applicable to similarly sized latex particles.[30−34] The fast aggregation rate coefficient (k^{fast}), which refers to the aggregation rate in unstable dispersions, was determined to be 3.08×10^{-18} m^3/s at a high salt concentration.

The colloidal stability was expressed in terms of stability ratio (W), which was calculated from the aggregation rate values as follows:

$$W = \frac{k^{fast}}{k} \quad (3)$$

One can realize that $W = 1$ is associated with unstable dispersions, where all particle collisions result in dimer formation.

Electrophoresis. Electrophoretic mobilities were measured on a Litesizer 500 instrument (Anton Paar) equipped with a 40 mW semiconductor laser of 658 nm wavelength operating in the backscattering mode at a scattering angle of 175°. For the determination of the electrophoretic mobilities, 5 mL samples were prepared. In brief, a 0.5 mL particle dispersion of 100 mg/L concentration was added to 4.5 mL of solution composed of the enzyme and/or NaCl at appropriate concentrations. The samples were allowed to rest 2 h at room temperature before measuring the electrophoretic mobilities, which occurred after 1 min equilibration time in the device. The reported values were the average of five individual measurements. The experiments were performed in 350 μL volume Ω-shaped plastic cuvettes (Anton Paar). The electrophoretic mobilities (u) were converted to ζ potential by Smoluchowski's equation as[35]

$$\zeta = \frac{u\eta}{\varepsilon_0 \varepsilon} \quad (4)$$

where ε is the relative permittivity of water, ε_0 is the permittivity of the vacuum, and η is the viscosity of the water. These values are 78.5, 8.9×10^{-12} F/m, and 8.9×10^{-4} Pas, respectively, in water and at the temperature used.

Hydrolytic Activity Measurements. For the determination of the protease-like activity, the "Universal Protease Activity Assay" protocol (Sigma-Aldrich) based on the Lowry method was used.[36] Accordingly, a calibration curve was measured by adding a different amount of 1.1 mM standard tyrosine solution in several samples and completing a final volume of 2 mL with ultrapure water. Tyrosine serves as the product of the hydrolysis in the test reaction, and its concentration range was 0.055−0.550 μM during calibration. After 30 min incubation at 37 °C, the solutions had a gradation of color correlating with the amount of tyrosine added. The UV−visible spectra of the obtained solutions were recorded on a Thermo Fischer Genesys 10S spectrophotometer. The absorbances at 660 nm were read and used to determine the tyrosine concentration. The protease-like activity experiments were carried out at 37 °C, and phosphate or acetate buffers were used to adjust the pH to 7.5 or 4.0, respectively, as detailed below.

During the measurements, 5 mL of 0.65 wv% casein as a substrate was diluted with 50 mM phosphate buffer solution first. A mixture consisting of 10 mM sodium acetate buffer and 5 mM calcium(II) was used to dilute the free or the immobilized enzyme solutions to reach an enzyme concentration of 0.1 U/mL. The volume of the free or the immobilized enzyme added to a 5 mL casein solution was varied to run the probe at different papain concentrations. The reaction was stopped after 10 min by adding 5 mL of 110 mM TCA solution, and then, an appropriate volume of enzyme solution was added to each tube to reach 1 mL of the final volume for the enzyme solutions in each tube. After 30 min of incubation, 2 mL of samples were filtered with a 0.45 μm syringe filter (Millex), and 5 mL of 500 mM sodium carbonate and 1 mL of 0.5 M Folin & Ciocalteu's reagent were added. The samples were then incubated again for 30 min. Thereafter, 2 mL of aliquots were filtered, and the absorbance was recorded. One unit of protease activity was equivalent to the amount of enzyme that required releasing 1 μg of tyrosine/mL/min under standard assay conditions described above.

Radical Scavenging Activity. The DPPH radical scavenging activity was determined as reported earlier,[37] with a slight modification. In the stock solutions of the free or immobilized enzymes, the concentration of the papain was 1000 ppm. The varying volume of enzyme stock was added to 1 mL of 12 mg/L DPPH solution dissolved in methanol and completed with water to a final volume of 2 mL. The enzyme content of the samples was ranged between 50 and 500 ppm. After short, vigorous stirring, the absorbance of the mixture was measured at 517 nm, which is the wavelength of the characteristic visible band of the DPPH. The absorbance values were followed for 1 h to detect the decrease in the initial DPPH concentration upon its reduction by the papain. In the case of the immobilized papain, after the 1 h reaction time, the samples were centrifuged for 10 min at 10 000 rpm to remove the particles from the samples in order to avoid any light scattering events during the spectrophotometric measurement. The decrease in the DPPH concentration was expressed as follows:

$$\text{DPPH}\ (\%) = \frac{A}{A_0}100 \quad (5)$$

where A is the absorbance measured after 1 h and A_0 is the absorbance value at the beginning of the test reaction.

RESULTS AND DISCUSSION

Papain Adsorption. Charging and aggregation properties of the sulfate latex particles were explored by electrophoresis and time-resolved DLS at different papain doses. The main goal was to find the optimal experimental conditions, where stable dispersions of enzyme−latex hybrid particles can be obtained. The pH of the samples was always kept at 4.0, and the dispersions contained 1 mM NaCl as a background electrolyte. The pH is below the pI of the enzyme;[38] therefore, papain was oppositely charged than that of latex due to the ionization of the sulfate groups present on the particle surface. Besides, these experimental conditions were selected due to the fact that the papain enzyme is used particularly in food and beer processing at a low pH.[14] The ζ potentials recorded at various papain concentrations are shown in Figure 2a.

DOI: 10.1021/acs.jpcb.9b08799
J. Phys. Chem. B 2019, 123, 9984−9991

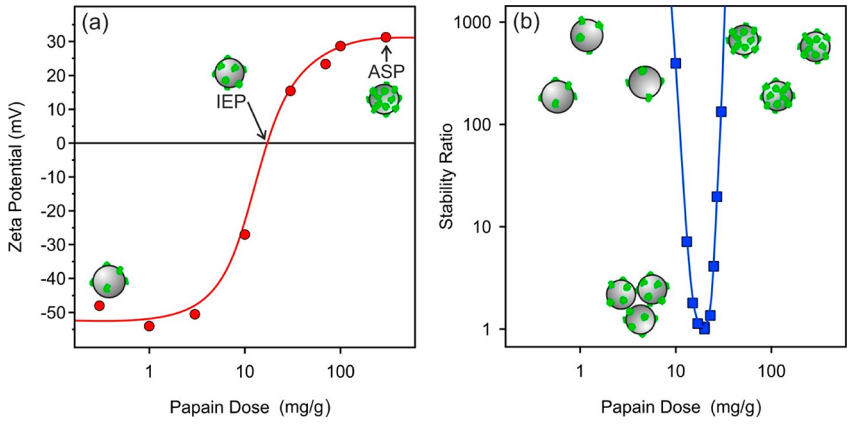

Figure 2. (a) ζ potential and (b) stability ratio data of the sulfate latex particles as a function of the papain dose used to functionalize the particles. The measurements were carried out at pH 4.0 and 1 mM ionic strength adjusted by NaCl. The mg/g unit refers to mg of papain per 1 g of latex. The solid lines serve to guide the eyes.

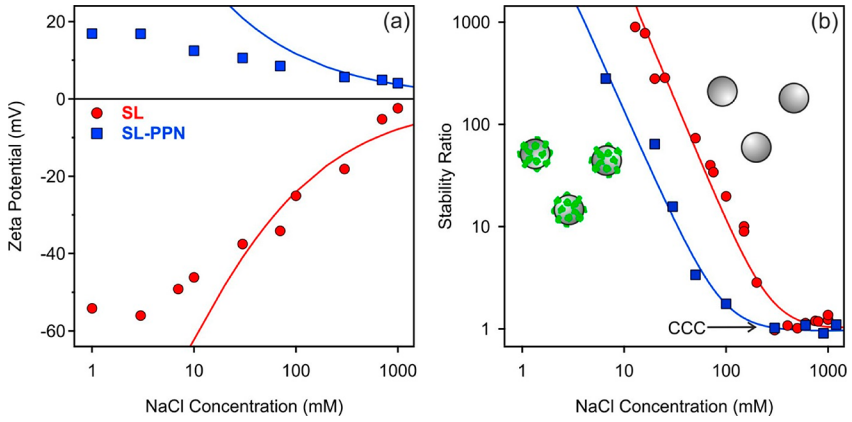

Figure 3. (a) ζ potential and (b) stability ratio values of the SL and SL-PPN (400 mg of enzyme adsorbed on 1 g of latex) particles as a function of the ionic strength adjusted by NaCl. The solid lines are data calculated with eqs 6 and 8 in panels a and b, respectively.

In general, the ζ potentials changed from negative to positive by increasing the added amount of papain, indicating its strong affinity to the oppositely charged particle surface. The potentials were negative at low doses, since the small amount of added enzyme compensated the surface charge of the particles only to a small extent. A further increase in the papain concentration led to charge neutralization at intermediate doses at the isoelectric point (IEP). The IEP is located at 20 mg/g. The adsorption process continued at doses higher than the IEP, and charge reversal of the particles occurred. At the highest doses applied, the ζ potentials reached a plateau with an onset at around a 400 mg/g dose. The potentials were close to +30 mV at this plateau. Accordingly, the coated latex possesses a significantly lower magnitude of ζ potential than the one for the bare particles (−55 mV), indicating a lower surface charge density for the former one. Papain added after the onset of the plateau remained dissolved in the solution. Such a charging behavior resembles the data determined earlier in oppositely charged particle−polyelectrolyte systems.[39−42] The driving forces causing the reversal in the sign of the surface charge in the adsorption process were identified as entropy gain due to solvent release upon adsorption, hydrophobic, and electrostatic interactions.[42−45]

Time-resolved DLS measurements were carried to determine stability ratio values under identical experimental conditions (i.e., particle concentration, pH, ionic strength, and papain dose range were the same) as in the electrophoretic study discussed above. The dependence of the stability ratios on the papain concentration is shown in Figure 2b.

The particles were stable, and no aggregation was detected at low and high enzyme doses, as indicated by high or not even measurable stability ratios. In the intermediate regime, however, the stability ratios formed a U-shaped curve with a minimum near the polyelectrolyte dose corresponding to the IEP determined in the ζ potential measurements. The stability ratios were unity within the experimental error at this minimum, indicating rapid particle aggregation and unstable dispersions. This behavior can be qualitatively explained by the theory developed by Derjaguin, Landau, Verwey, and Overbeek (DLVO),[46−48] and it is similar to that experienced earlier in systems containing colloidal particles and oppositely charged species such as multivalent ions[32,49,50] and polyelectrolytes.[11,33,40,45] The latex particles possessed sufficient charge at low and high doses, as indicated by the relatively high magnitude of the ζ potentials, and the repulsive electrical double-layer forces stabilized the dispersions. At the IEP, where the adsorbed papain neutralized the charge of the sulfate latex, the electrical double layers vanished due to the lack of surface charge, and thus, the attractive van der Waals forces destabilized the dispersions. The presence of other types of interparticle forces, such as patch-charge,[51] steric,[52] or bridging interactions,[53] which may be present in particle−polymer

DOI: 10.1021/acs.jpcb.9b08799
J. Phys. Chem. B 2019, 123, 9984−9991

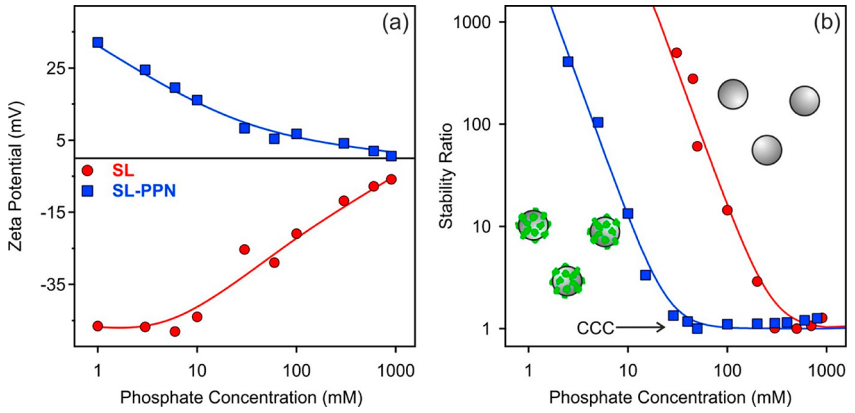

Figure 4. (a) ζ potential and (b) stability ratio values of the SL and SL-PPN (400 mg of enzyme adsorbed on 1 g of latex) particles as a function of the phosphate concentration at pH 4.0. The solid lines are eye guides in panel a and calculated by eq 8 in panel b.

systems,[54−56] could not be detected on the basis of the above experimental results.

From these findings, one can conclude that papain adsorption at a dose of 400 mg/g gave rise to the formation of an enzyme layer on the latex surface (these particles will be denoted as SL-PPN later). Moreover, the obtained SL-PPN hybrid possessed excellent colloidal stability; i.e., highly stable dispersions of primary particles were present in the samples at the experimental conditions applied.

Resistance against Salt-Induced Aggregation. Given the fact that immobilized enzymes are often used in liquid environments containing electrolytes or even their mixtures, the resistance of the SL-PPN hybrid against salt-induced aggregation was tested and compared with the bare sulfate latex particles (SL). Prior to the aggregation study, the charging characteristics were assessed by determining the ζ potentials at different ionic strengths (Figure 3a).

The magnitude of the potentials decreased with the NaCl concentration in both cases, owing to the screening effect of the electrolyte on the surface charge. However, the decrease was higher for the SL particles due to their elevated ζ potentials at low ionic strengths, as discussed earlier. The potentials did not change the sign in the entire ionic strength range investigated. To determine the charge density (σ), the Grahame equation was used:[48]

$$\sigma = \frac{2k_B T\varepsilon_0\varepsilon\kappa}{e}\sin h\left[\frac{e\zeta}{2k_B T}\right] \tag{6}$$

where k_B is the Boltzmann constant, T is the temperature, e is the elementary charge, and κ is the inverse Debye length, which can be calculated from the ionic strength (I) as[35]

$$\kappa = \left(\frac{2N_A e^2 I}{\varepsilon\varepsilon_0 k_B T}\right)^{1/2} \tag{7}$$

where N_A is the Avogadro number. Due to the fact that ζ potential is applied in eq 6, the surface charge at the slip plane was estimated by this model. The determined surface charge densities were 8 mC/m^2 and −18 mC/m^2 for the SL-PPN and SL, respectively. Such a lower magnitude of the charge density for the enzyme-coated latex most likely originates from counterion condensation phenomenon, which takes place for charged macromolecules in the electrolyte medium, leading to lower effective charges.[57]

The absolute aggregation rates of the SL and SL-PPN particles were determined at a high salt concentration, where the double-layer forces are screened and the particles rapidly aggregate. The values were found to be 3.3×10^{-18} m^3/s and 3.1×10^{-18} m^3/s for SL-PPN and SL, respectively. These data indicate that the nature of the attractive forces are very similar for both particles, and they originate most probably from van der Waals interactions, similar to other polyelectrolyte-coated latexes.[34] Figure 3b shows the stability ratios determined for SL and SL-PPN at different salt levels using eq 3.

Slow aggregation was observed at low ionic strengths, and unstable suspensions were detected at high NaCl concentrations in line with the prediction by the DLVO theory, i.e., the electrical double-layer forces disappear above the critical coagulation concentration (CCC), which was determined as[58]

$$W = 1 + \left[\frac{\mathrm{CCC}}{c}\right]^{\beta} \tag{8}$$

where c is the salt concentration and β was obtained from the change in the stability ratios in the slow aggregation regime before the CCC as

$$\beta = \frac{\mathrm{d}\log 1/W}{\mathrm{d}\log c} \tag{9}$$

Note that the above equations are empirical formulas to fit the stability ratio data at different NaCl concentrations and to obtain the CCC values. The different surface charge densities were reflected in the CCCs, and the bare SL possesses a higher CCC value of 270 mM compared to the 90 mM for SL-PPN. These data were calculated with eq 8. This decrease upon papain adsorption can be explained by the lower charge density and, hence, by the weaker double-layer forces acting between the SL-PPN particles.

Due to the fact that phosphate ions are often present during the applications of the papain enzyme, the colloidal stability of SL and SL-PPN particles was investigated in the presence of phosphate ions too. Similar conditions were used like in the case of NaCl-induced aggregation, and the phosphate ions are present 99% in the dihydrogen phosphate form; i.e., they are monovalent ions, at pH 4.0.[59] The magnitude of the ζ potentials decreased with the phosphate concentration for both particles due to the progressive charge screening by the ionic environment and the possible specific adsorption of the phosphate ions in the case of the positively charged SL-PPN (Figure 4a).[32]

DOI: 10.1021/acs.jpcb.9b08799
J. Phys. Chem. B 2019, 123, 9984−9991

The aggregation behaviors in the presence of phosphate resemble the ones with NaCl discussed above. Slow and fast aggregation regimes are separated by well-defined CCC, which is similar (280 mM) to the CCC of the bare SL measured in the presence of NaCl. However, the CCC values varied for the SL-PPN in a different ionic environment, and 25 mM was determined with phosphate ions, which is significantly lower than the one determined in NaCl solutions. This decrease may come from the specific adsorption of phosphate ions[32] and subsequent weakening of the double-layer forces. Since the stability ratios were in unity within the experimental error above the CCC, the presence of additional (non-DLVO) forces, such as bridging through adsorbed phosphate ions, was excluded.

Besides, another important fact is that in the case of SL-PPN, the ζ potentials are very low even before the CCC, where stable dispersions were detected. This result clearly indicates that the stabilizing forces are not only of electrostatic origin for the enzyme-coated particles. Since the bare SL behave as predicted by the DLVO theory, this additional stabilizing effect must come from the adsorbed papain chains, which overlap upon the approach of two particles, and an osmotic pressure arises, leading to repulsive forces. This so-called steric stabilization was reported earlier with polymer-functionalized colloidal particles;[6,24,52] nevertheless, one can observe them only with latex particles of a papain monolayer on the surface and not at partial coverage in the present system.

Protease-like Function. The hydrolytic activity of the free and immobilized papain was estimated on the basis of the hydrolysis of the casein substrate, as detailed in the Experimental Section. The time-dependent enzymatic assay was investigated by recording the characteristic absorbance of the tyrosine product at a 660 nm wavelength. As shown in Figure 5a and b, the absorbance values increased with the reaction time for both the free and the immobilized enzyme. However, the increase was more pronounced for the free papain. By calculating the normalized activities, 0.28 U/mL and 0.19 U/mL were obtained for the papain and SL-PPN, respectively. These numbers indicate that the enzyme lost from its activity upon immobilization, most likely due to some conformational changes, which occurred once it was attached to the surface of the latex. Indeed, it was also reported earlier that enzymes may change their conformation, resulting in a loss of activity.[60] Such a change may result in decreased activity due to the hindered interaction between the active center and the substrate. Another reason for this decrease can be the relatively high absorbed amount (400 mg/g) of the enzyme. Accordingly, the papain absorbed on the surface in more than one layer and the blocking effect of the outer layers, i.e., the limited accessibility of substrate molecules to the inner layers, decrease the efficiency. The third reason is in connection with the free enzyme in solution, where the free movement of the papain eases the collision with the substrate, while the immobilized one diffuses slower, and thus, it approaches fewer target molecules.

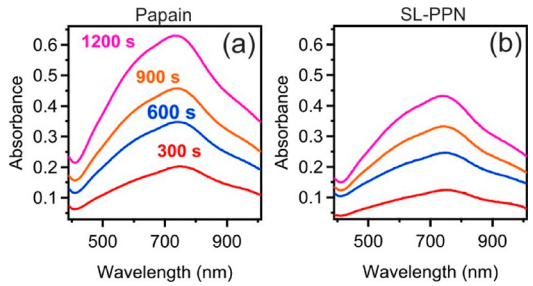

Figure 5. Time-dependent UV−visible spectra recorded during protease-like activity measurements with the (a) free papain and (b) SL-PPN. The applied papain dose was 3 ppm for both the free and immobilized enzymes.

Although the enzymatic activity in the SL-PPN decreased compared to the native enzyme in homogeneous solution, the hybrid maintains significant protease-like activity. Considering these facts and also the advantages gained by the immobilization (e.g., better separation from the reaction mixture), the obtained SL-PPN hybrid is a promising candidate as a biocatalyst in hydrolytic processes.

Radical Scavenging Activity. The antioxidant activity of the papain enzyme has been reported in the literature;[17] however, no results on the antioxidant activity of the immobilized papain have been published yet. The DPPH radical scavenging assay has been widely used to evaluate the antioxidant properties of various antioxidants.[37] The DPPH content of the samples was followed by a spectrophotometer, and the decrease in % was calculated with eq 5. These values were plotted versus the enzyme concentration, and the EC_{50} values were determined (Figure 6).

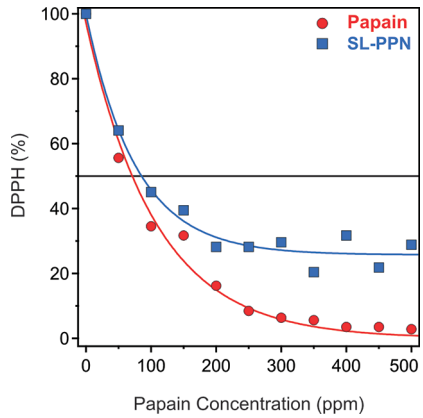

Figure 6. DPPH scavenging activity of the free papain and the SL-PPN expressed by the change in the substrate concentrations as a function of the enzyme dose. The lines are eye guides.

The EC_{50} represents the enzyme concentration, at which the initial DPPH concentration decreased to half; i.e., 50% of the radicals are scavenged by the antioxidant materials. The activity of the SL-PPN was determined as 85.4 ppm compared to the free enzyme, whose EC_{50} was 71.1 ppm. Accordingly, a decrease was experienced in the activity upon immobilization of the enzyme due to most likely the same reasons discussed above for the protease-like activity. Nevertheless, these results clearly indicate that the SL-PPN possesses remarkable antioxidant activity.

Considering the values reported above to quantify the different functions of the free enzyme and SL-PPN, one can conclude that the hydrolytic and antioxidant activities of papain decreased by 32% and 20%, respectively, upon immobilization. However, the enzymatic tests all together shed light on the fact that the hybrid materials is an excellent candidate in applications, where biocatalysts of hydrolytic and antioxidant activities are required in heterogeneous systems.

DOI: 10.1021/acs.jpcb.9b08799
J. Phys. Chem. B 2019, 123, 9984−9991

CONCLUSIONS

The colloidal behavior of sulfate latex and its papain modified forms was studied through assessment of the charging and aggregation properties in a wide range of experimental conditions. The papain enzyme strongly adsorbed on the oppositely charged sulfate latex surface, mainly through electrostatic forces. The adsorption process resulted in charge neutralization at the intermediate and charge reversal at higher papain doses. The formation of an enzyme monolayer on the surface resulted in stable papain−latex dispersions, while unstable samples were observed at enzyme doses close to the charge neutralization point. The major interparticle forces were described within the DLVO theory; however, steric interactions between adsorbed enzyme chains and subsequent stabilization of the particles occurred at high papain coverage. The hydrolytic and antioxidant activity of the papain-coated latex was estimated, and they were slightly lower for the immobilized enzyme than for the free papain. Nevertheless, the obtained papain−latex hybrid material possesses the advantages of a heterogeneous catalyst such as easier separation from the reaction mixture, and thus, it can be used as a multifunctional material, for instance, in the food industry, where joint protease-like and antioxidant functions are welcome in several processes.

AUTHOR INFORMATION

Corresponding Author

*E-mail: szistvan@chem.u-szeged.hu.

ORCID

Istvan Szilagyi: 0000-0001-7289-0979

Notes

The authors declare no competing financial interest.

ACKNOWLEDGMENTS

Financial support by the Lendület program of the Hungarian Academy of Sciences (96130) and by the Ministry of Human Capacities Hungary (20391-3/2018/FEKUSTRAT) is gratefully acknowledged.

REFERENCES

(1) DiCosimo, R.; McAuliffe, J.; Poulose, A. J.; Bohlmann, G. Industrial use of immobilized enzymes. *Chem. Soc. Rev.* **2013**, *42*, 6437−6474.

(2) Popat, A.; Hartono, S. B.; Stahr, F.; Liu, J.; Qiao, S. Z.; Lu, G. Q. Mesoporous silica nanoparticles for bioadsorption, enzyme immobilisation, and delivery carriers. *Nanoscale* **2011**, *3*, 2801−2818.

(3) Bosio, V. E.; Islan, G. A.; Martinez, Y. N.; Duran, N.; Castro, G. R. Nanodevices for the immobilization of therapeutic enzymes. *Crit. Rev. Biotechnol.* **2016**, *36*, 1−18.

(4) Sheldon, R. A.; van Pelt, S. Enzyme immobilisation in biocatalysis: Why, what and how. *Chem. Soc. Rev.* **2013**, *42*, 6223−6235.

(5) Chang, F. P.; Chen, Y. P.; Mou, C. Y. Intracellular implantation of enzymes in hollow silica nanospheres for protein therapy: Cascade system of Superoxide Dismutase and Catalase. *Small* **2014**, *10*, 4785−4795.

(6) Pavlovic, M.; Rouster, P.; Szilagyi, I. Synthesis and formulation of functional bionanomaterials with superoxide dismutase activity. *Nanoscale* **2017**, *9*, 369−379.

(7) Demeter, E. L.; Hilburg, S. L.; Washburn, N. R.; Collins, T. J.; Kitchin, J. R. Electrocatalytic oxygen evolution with an immobilized TAML activator. *J. Am. Chem. Soc.* **2014**, *136*, 5603−5606.

(8) Bartha-Vari, J. H.; Tosa, M. I.; Irimie, F. D.; Weiser, D.; Boros, Z.; Vertessy, B. G.; Paizs, C.; Poppe, L. Immobilization of phenylalanine ammonia-lyase on single-walled carbon nanotubes for stereoselective biotransformations in batch and continuous-flow modes. *ChemCatChem* **2015**, *7*, 1122−1128.

(9) Planchestainer, M.; Contente, M. L.; Cassidy, J.; Molinari, F.; Tamborini, L.; Paradisi, F. Continuous flow biocatalysis: production and in-line purification of amines by immobilised transaminase from Halomonas elongata. *Green Chem.* **2017**, *19*, 372−375.

(10) Welsch, N.; Wittemann, A.; Ballauff, M. Enhanced activity of enzymes immobilized in thermoresponsive core-shell microgels. *J. Phys. Chem. B* **2009**, *113*, 16039−16045.

(11) Rouster, P.; Pavlovic, M.; Saringer, S.; Szilagyi, I. Functionalized titania nanosheet dispersions of peroxidase activity. *J. Phys. Chem. C* **2018**, *122*, 11455−11463.

(12) Fan, Y. M.; Cao, X. D.; Hu, T.; Lin, X. G.; Dong, H.; Zou, X. N. Enhancement of enzymatic activity using microfabricated poly-(epsilon-caprolactone)/silica hybrid microspheres with hierarchically porous architecture. *J. Phys. Chem. C* **2016**, *120*, 3955−3963.

(13) Kudina, O.; Zakharchenko, A.; Trotsenko, O.; Tokarev, A.; Ionov, L.; Stoychev, G.; Puretskiy, N.; Pryor, S. W.; Voronov, A.; Minko, S. Highly efficient phase boundary biocatalysis with enzymogel nanoparticles. *Angew. Chem., Int. Ed.* **2014**, *53*, 483−487.

(14) Fernandez-Lucas, J.; Castaneda, D.; Hormigo, D. New trends for a classical enzyme: Papain, a biotechnological success story in the food industry. *Trends Food Sci. Technol.* **2017**, *68*, 91−101.

(15) Drenth, J.; Jansonius, J. N.; Koekoek, R.; Swen, H. M.; Wolthers, B. G. Structure of papain. *Nature* **1968**, *218*, 929−932.

(16) Kamphuis, I. G.; Kalk, K. H.; Swarte, M. B. A.; Drenth, J. Structure of papain refined at 1.65 A resolution. *J. Mol. Biol.* **1984**, *179*, 233−256.

(17) Liu, M. C.; Yang, S. J.; Hong, D.; Yang, J. P.; Liu, M.; Lin, Y.; Huang, C. H.; Wang, C. J. A simple and convenient method for the preparation of antioxidant peptides from walnut (Juglans regia L.) protein hydrolysates. *Chem. Cent. J.* **2016**, *10*, 39.

(18) Alpay, P.; Uygun, D. A. Usage of immobilized papain for enzymatic hydrolysis of proteins. *J. Mol. Catal. B: Enzym.* **2015**, *111*, 56−63.

(19) Zou, N.; Plank, J. Intercalation of papain enzyme into hydrotalcite type layered double hydroxide. *J. Phys. Chem. Solids* **2012**, *73*, 1127−1130.

(20) Dai, H. J.; Ou, S. Y.; Liu, Z. J.; Huang, H. H. Pineapple peel carboxymethyl cellulose/polyvinyl alcohol/mesoporous silica SBA-15 hydrogel composites for papain immobilization. *Carbohydr. Polym.* **2017**, *169*, 504−514.

(21) Mahmoud, K. A.; Lam, E.; Hrapovic, S.; Luong, J. H. T. Preparation of well-dispersed gold/magnetite nanoparticles embedded on cellulose nanocrystals for efficient immobilization of papain enzyme. *ACS Appl. Mater. Interfaces* **2013**, *5*, 4978−4985.

(22) Szabo, T.; Szekeres, M.; Dekany, I.; Jackers, C.; De Feyter, S.; Johnston, C. T.; Schoonheydt, R. A. Layer-by-layer construction of ultrathin hybrid films with proteins and clay minerals. *J. Phys. Chem. C* **2007**, *111*, 12730−12740.

(23) Lopez-Leon, T.; Santander-Ortega, M. J.; Ortega-Vinuesa, J. L.; Bastos-Gonzalez, D. Hofmeister effects in colloidal systems: Influence of the surface nature. *J. Phys. Chem. C* **2008**, *112*, 16060−16069.

(24) Vasti, C.; Bedoya, D. A.; Rojas, R.; Giacomelli, C. E. Effect of the protein corona on the colloidal stability and reactivity of LDH-based nanocarriers. *J. Mater. Chem. B* **2016**, *4*, 2008−2016.

(25) Moore, T. L.; Rodriguez-Lorenzo, L.; Hirsch, V.; Balog, S.; Urban, D.; Jud, C.; Rothen-Rutishauser, B.; Lattuada, M.; Petri-Fink, A. Nanoparticle colloidal stability in cell culture media and impact on cellular interactions. *Chem. Soc. Rev.* **2015**, *44*, 6287−6305.

(26) Cobbe, S.; Connolly, S.; Ryan, D.; Nagle, L.; Eritja, R.; Fitzmaurice, D. DNA-controlled assembly of protein-modified gold nanocrystals. *J. Phys. Chem. B* **2003**, *107*, 470−477.

(27) Yang, T.; Li, Z.; Wang, L.; Guo, C. L.; Sun, Y. J. Synthesis, characterization, and self-assembly of protein lysozyme monolayer-stabilized gold nanoparticles. *Langmuir* **2007**, *23*, 10533−10538.

DOI: 10.1021/acs.jpcb.9b08799
J. Phys. Chem. B 2019, 123, 9984−9991

(28) Hassan, P. A.; Rana, S.; Verma, G. Making sense of Brownian motion: Colloid characterization by dynamic light scattering. *Langmuir* **2015**, *31*, 3−12.
(29) Berne, B. J.; Pecora, R. *Dynamic light scattering*; Robert E. Krieger Publishing: Malabar, 1990.
(30) Trefalt, G.; Szilagyi, I.; Oncsik, T.; Sadeghpour, A.; Borkovec, M. Probing colloidal particle aggregation by light scattering. *Chimia* **2013**, *67*, 772−776.
(31) Holthoff, H.; Egelhaaf, S. U.; Borkovec, M.; Schurtenberger, P.; Sticher, H. Coagulation rate measurements of colloidal particles by simultaneous static and dynamic light scattering. *Langmuir* **1996**, *12*, 5541−5549.
(32) Sugimoto, T.; Cao, T. C.; Szilagyi, I.; Borkovec, M.; Trefalt, G. Aggregation and charging of sulfate and amidine latex particles in the presence of oxyanions. *J. Colloid Interface Sci.* **2018**, *524*, 456−464.
(33) Hierrezuelo, J.; Vaccaro, A.; Borkovec, M. Stability of negatively charged latex particles in the presence of a strong cationic polyelectrolyte at elevated ionic strengths. *J. Colloid Interface Sci.* **2010**, *347*, 202−208.
(34) Hierrezuelo, J.; Sadeghpour, A.; Szilagyi, I.; Vaccaro, A.; Borkovec, M. Electrostatic Stabilization of Charged Colloidal Particles with Adsorbed Polyelectrolytes of Opposite Charge. *Langmuir* **2010**, *26*, 15109−15111.
(35) Delgado, A. V.; Gonzalez-Caballero, F.; Hunter, R. J.; Koopal, L. K.; Lyklema, J. Measurement and interpretation of electrokinetic phenomena. *J. Colloid Interface Sci.* **2007**, *309*, 194−224.
(36) Cupp-Enyard, C. Sigma's non-specific protease activity assay - Casein as a substrate. *J. Visualized Exp.* **2008**, *19*, e899.
(37) Brand-Williams, W.; Cuvelier, M. E.; Berset, C. Use of a free-radical method to evaluate antioxidant activity. *Food Sci. Technol.-Lebensm.-Wiss. Technol.* **1995**, *28*, 25−30.
(38) Sahoo, B.; Sahu, S. K.; Bhattacharya, D.; Dhara, D.; Pramanik, P. A novel approach for efficient immobilization and stabilization of papain on magnetic gold nanocomposites. *Colloids Surf., B* **2013**, *101*, 280−289.
(39) Hyde, E. D. E.; Moreno-Atanasio, R.; Millner, P. A.; Neville, F. Surface charge control through the reversible adsorption of a biomimetic polymer on silica particles. *J. Phys. Chem. B* **2015**, *119*, 1726−1735.
(40) Iselau, F.; Xuan, T. P.; Trefalt, G.; Matic, A.; Holmberg, K.; Bordes, R. Formation and relaxation kinetics of starch-particle complexes. *Soft Matter* **2016**, *12*, 9509−9519.
(41) Cherstvy, A. G.; Winkler, R. G. Simple model for overcharging of a sphere by a wrapped oppositely charged asymmetrically neutralized polyelectrolyte: Possible effects of helical charge distribution. *J. Phys. Chem. B* **2005**, *109*, 2962−2969.
(42) Borkovec, M.; Papastavrou, G. Interactions between solid surfaces with adsorbed polyelectrolytes of opposite charge. *Curr. Opin. Colloid Interface Sci.* **2008**, *13*, 429−437.
(43) Quesada-Perez, M.; Gonzalez-Tovar, E.; Martin-Molina, A.; Lozada-Cassou, M.; Hidalgo-Alvarez, R. Overcharging in colloids: Beyond the Poisson-Boltzmann approach. *ChemPhysChem* **2003**, *4*, 234−248.
(44) Carrillo, J. Y.; Dobrynin, A. V. Molecular dynamics simulations of polyelectrolyte adsorption. *Langmuir* **2007**, *23*, 2472−2482.
(45) Szilagyi, I.; Trefalt, G.; Tiraferri, A.; Maroni, P.; Borkovec, M. Polyelectrolyte adsorption, interparticle forces, and colloidal aggregation. *Soft Matter* **2014**, *10*, 2479−2502.
(46) Derjaguin, B.; Landau, L. D. Theory of the stability of strongly charged lyophobic sols and of the adhesion of strongly charged particles in solutions of electrolytes. *Acta Phys. Chim.* **1941**, *14*, 633−662.
(47) Verwey, E. J. W.; Overbeek, J. T. G. *Theory of stability of lyophobic colloids*; Elsevier: Amsterdam, 1948.
(48) Israelachvili, J. *Intermolecular and surface forces*, 3rd ed.; Academic Press: London, 2011.
(49) Cao, T. C.; Sugimoto, T.; Szilagyi, I.; Trefalt, G.; Borkovec, M. Heteroaggregation of oppositely charged particles in the presence of multivalent ions. *Phys. Chem. Chem. Phys.* **2017**, *19*, 15160−15171.
(50) Sinha, P.; Szilagyi, I.; Ruiz-Cabello, F. J. M.; Maroni, P.; Borkovec, M. Attractive forces between charged colloidal particles induced by multivalent ions revealed by confronting aggregation and direct force measurements. *J. Phys. Chem. Lett.* **2013**, *4*, 648−652.
(51) Leong, Y. K. Interparticle forces arising from an adsorbed strong polyelectrolyte in colloidal dispersions: charged patch attraction. *Colloid Polym. Sci.* **1999**, *277*, 299−305.
(52) Fritz, G.; Schadler, V.; Willenbacher, N.; Wagner, N. J. Electrosteric stabilization of colloidal dispersions. *Langmuir* **2002**, *18*, 6381−6390.
(53) Brunel, F.; Pochard, I.; Gauffinet, S.; Turesson, M.; Labbez, C. Structure and yielding of colloidal silica gels varying the range of interparticle interactions. *J. Phys. Chem. B* **2016**, *120*, 5777−5785.
(54) Feng, L. L.; Stuart, M. C.; Adachi, Y. Dynamics of polyelectrolyte adsorption and colloidal flocculation upon mixing studied using mono-dispersed polystyrene latex particles. *Adv. Colloid Interface Sci.* **2015**, *226*, 101−114.
(55) Meng, Z. Y.; Hashmi, S. M.; Elimelech, M. Aggregation rate and fractal dimension of fullerene nanoparticles via simultaneous multiangle static and dynamic light scattering measurement. *J. Colloid Interface Sci.* **2013**, *392*, 27−33.
(56) Saringer, S.; Rouster, P.; Szilagyi, I. Regulation of the stability of titania nanosheet dispersions with oppositely and like-charged polyelectrolytes. *Langmuir* **2019**, *35*, 4986−4994.
(57) Manning, G. S. Limiting laws and counterion condensation in polyelectrolyte solutions 1. Colligative properties. *J. Chem. Phys.* **1969**, *51*, 924−933.
(58) Grolimund, D.; Elimelech, M.; Borkovec, M. Aggregation and deposition kinetics of mobile colloidal particles in natural porous media. *Colloids Surf., A* **2001**, *191*, 179−188.
(59) May, P. M.; Rowland, D.; Konigsberger, E.; Hefter, G. JESS, a Joint Expert Speciation System - IV: A large database of aqueous solution physicochemical properties with an automatic means of achieving thermodynamic consistency. *Talanta* **2010**, *81*, 142−148.
(60) Krajewska, B. Application of chitin- and chitosan-based materials for enzyme immobilizations: a review. *Enzyme Microb. Technol.* **2004**, *35*, 126−139.

DOI: 10.1021/acs.jpcb.9b08799
J. Phys. Chem. B 2019, 123, 9984−9991